Available on CMS information server

CMS NOTE -2009/017

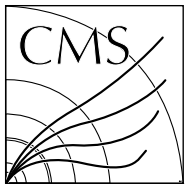

The Compact Muon Solenoid Experiment

CMS Note

Mailing address: CMS CERN, CH-1211 GENEVA 23, Switzerland

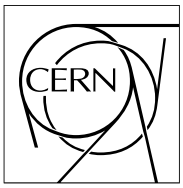

23 May 2009 (v4, 06 October 2009)

The Grounding and Shielding of the Tracker Inner Barrel and Disks (TIB/TID)

J. Bernardini[a)], C. Cerri[b)], R. D'Alessandro[c)], S. Mersi[c)], S. Paoletti[d)], A. Rizzi[a)+)], G. Sguazzoni[d)], A. Venturi[b)], M. Vos[b)*)]

Abstract

During the construction of the CMS silicon strip tracker, one of the issues addressed was that of the grounding and shielding of the detector. The complexity of the system was unprecedented, with many issues requiring careful consideration before a full solution could be found. In particular, the problems encountered and the solutions adopted for the silicon Tracker Inner Barrel and Disks (TIB/TID) will be described. Since this work the TIB/TID has been integrated with the rest of the CMS Tracker and has participated in cosmic ray studies, both above ground with the full Tracker and below ground with the full CMS detector. Throughout these studies the noise performance has been consistent with that of the as-delivered system.

[a)] Scuola Normale Superiore di Pisa and I.N.F.N. Sezione di Pisa

[b)] I.N.F.N. Sezione di Pisa

[c)] Università degli Studi di Firenze and I.N.F.N. Sezione di Firenze

[d)] I.N.F.N. Sezione di Firenze

[+)] Currently at ETH, Zurich

[*)] Currently at IFIC, Centro mixto U.Valencia/CSIC, Valencia, Spain

1 Introduction

The CMS Silicon Strip Tracker (SST) is now in its final check/out phase after having being extensively tested with cosmic rays. CMS lowered the whole SST at the end of 2007 and the detector is now cabled up and ready for the first beams from the LHC. The successful completion of the SST project (ongoing now for more than ten years) has been possible thanks to an enormous effort by hundreds of people from many institutions in the design and construction phase of the detector. In particular, the TIB/TID (Tracker Inner Barrel and Disks) was constructed by a collaboration of Italian universities and INFN laboratories, before being sent to CERN for final integration in the SST. Of the many problems that arose during the TIB/TID integration process, this note is focussed on what is probably the most critical aspect in dealing with silicon detectors: the grounding and shielding of the detector modules and the mechanical structure.

The modules used in the TIB/TID have been characterised by an excellent S/N ratio as consistently measured by all module test facilities [1]. Typical S/N ratios for MIPs are of the order of 20 to 30 depending on the FE chip configuration. Grounding and shielding, however, is concerned more with common mode noise, stemming from spurious pickups from external sources. These effects can jeopardize the performance of any assembly of high quality detectors. Also the effects can and will depend on the physical size of the assembly itself. Thus the need for a continuous monitoring of the performance and the need for new grounding and shielding prescriptions, as the TIB/TID evolved from the assembly of a few pieces on a test bench to a full fledged instrument of precision.

After a brief overview of the CMS silicon tracker, a detailed description of the Inner Barrel system is given. The TIB/TID performance is analysed with regards to the solutions adopted for the grounding and shielding of the system. Finally, the performance obtained after insertion in the Tracker support tube at CERN is reviewed.

2 The CMS silicon tracker

The CMS tracker is the largest silicon micro-strip detector ever designed. Consisting of three main sub-assemblies, TIB/TID (Tracker Inner Barrel, Tracker Inner Disks), TOB (Tracker Outer Barrel), and TEC (Tracker End Caps), it is $5.4\,\mathrm{m}$ long and is $2.4\,\mathrm{m}$ in diameter. The total surface area of the sensors comprising the 15232 modules is an unprecedented 198 m^2 [2]. Figure 1 is a schematic drawing of the various tracker volumes. Power and control signals are not distributed individually to the modules, instead they are grouped in power groups and control rings so as to drastically reduce the number of cables and fibres. A detailed description of the silicon strip tracker is given in [3], [4], and [5].

The CMS solenoid provides a homogeneous magnetic field of ~ 4T over the full volume of the tracker. The Tracker will be operated so that sensor temperatures will be at of slightly below $-10°$C. At the LHC design luminosity of $10^{34}\,\mathrm{cm}^{-2}\,\mathrm{sec}^{-1}$ there will be on average 1000 charged particles in the more than 20 proton-proton collisions per $25\,\mathrm{ns}$ bunch crossing. Even though the SST is an all silicon system with the same front end electronics (FE) and

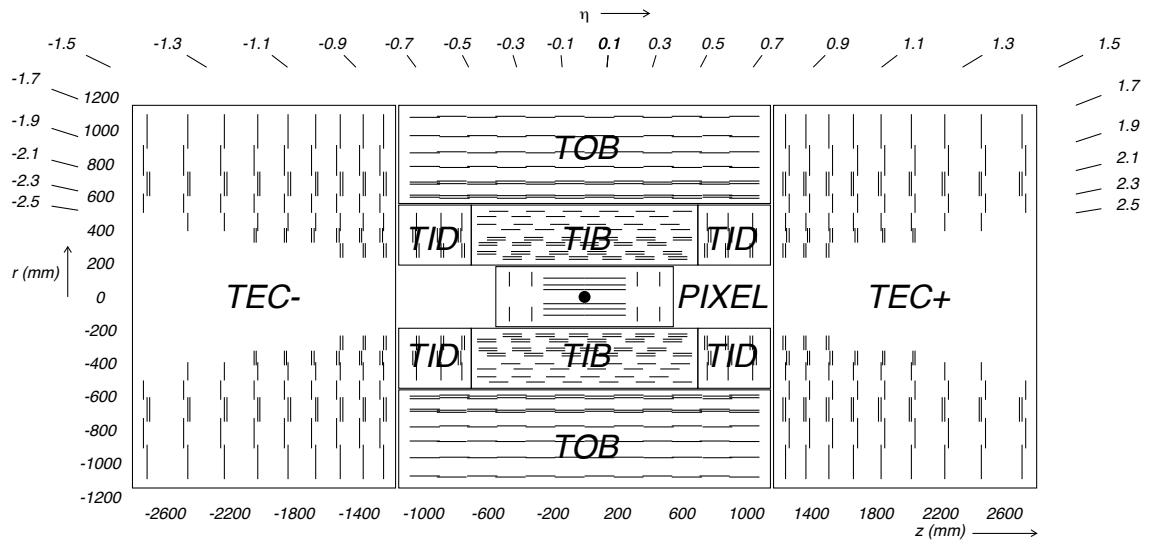

Figure 1: *Schematic cross-section of the CMS tracker. Each line represents a detector module. Double lines indicate back-to-back modules, which provide stereo information.*

same type of auxiliary chips everywhere, the three sub-systems have unique grounding and shielding requirements. The TIB/TID, in particular, uses aluminium for its cooling circuits and kapton circuits (*Mother Cables*) to connect modules together in groups of three (if the modules are single-sided) or six (in case of double-sided). Also the modules were integrated directly onto cylindrical half shells with no intermediate sub-structure.

2.1 The Tracker Inner Barrel/Disks Components

The Tracker Inner Barrel (TIB) consists of four concentric cylinders placed at $255.0\,\mathrm{mm}$, $339.0\,\mathrm{mm}$, $418.5\,\mathrm{mm}$, and $498.0\,\mathrm{mm}$ radius respectively from the beam axis, and extends from $-700\,\mathrm{mm}$ to $+700\,\mathrm{mm}$ along the z axis. The two innermost layers (Layer 1 and 2) host double-sided modules with a strip pitch of $80\,\mu\mathrm{m}$, while the other two layers (Layer 3 and 4) host single-sided modules with a strip pitch of $120\,\mu\mathrm{m}$. Each cylinder is subdivided into four sub-assemblies ($+z/-z$, up/down) for ease of handling and integration. Each of these sub-assemblies (shells) contains an independent array of services from cooling to electronics and thus can be fully equipped and tested before being mechanically coupled to each other during final assembly. Figure 2 shows a fully assembled TIB+.

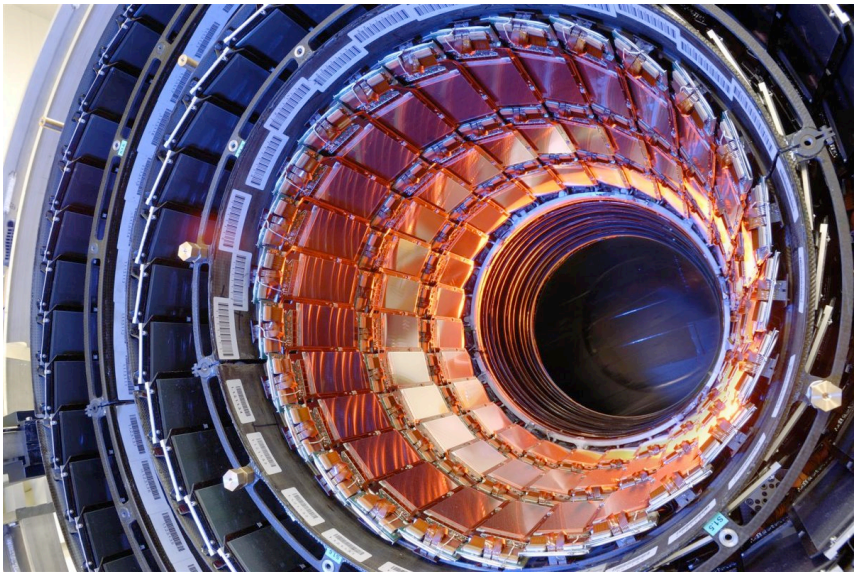

Figure 2: *Nested cylinders of the TIB+ as viewed from the TIB- side. Services come out at the other end. For each cylinder, modules are assembled both on the outer and inner surfaces, thus ensuring a hermetic coverage.*

Coupled at the end of the TIB+ and the TIB- (referred to as $+z$ or $-z$) are two service cylinders, which terminate at a service distribution disk (*margherita*). These service cylinders play a dual role: one is to route services from the shells to the *margherita*, the other is to support the Tracker Inner Disks (TID), which are placed inside them. Figure 3 shows a schematic drawing of one half TIB/TID structure together with its corresponding *margherita*. The shells, disks, and service cylinders are made of high strength, low deformation carbon fibre, chosen both for its lightness and its low material budget.

In contrast to the other mechanical components, the *margherita* is instead made of conventional FR-4 fibre epoxy with $30\,\mu\mathrm{m}$ gold-plated copper on both sides. Thus the *margherita* defines the outer boundary of the Faraday cage that encloses the TIB/TID, the other boundary being the protective shielding between TOB and TIB/TID. This choice allows for effective decoupling of cable shields, which are interrupted at this level and do not enter the sensitive tracker volume. The *margherita* supports all of the power and control cable connectors, which are mounted on its outer petals, while the optical fibre connectors are mounted on the innermost part. The cooling tubes run along the petals of the *margherita* and are in electrical contact with the structure. The silicon detector modules are mounted directly on the structure's cylinders and disks. Thus a large number of modules has to be integrated and tested at any one time.

2.2 Power supplies for the Silicon Strip Tracker

The tracker structures are powered by the CAEN EASY 3000 modular system [6]. Each power group is supplied by one "power supply unit" (PSU) featuring two low voltage (LV) regulators: $2.5\,\mathrm{V}$ (max current $13\mathrm{A}$) and $1.25\,\mathrm{V}$

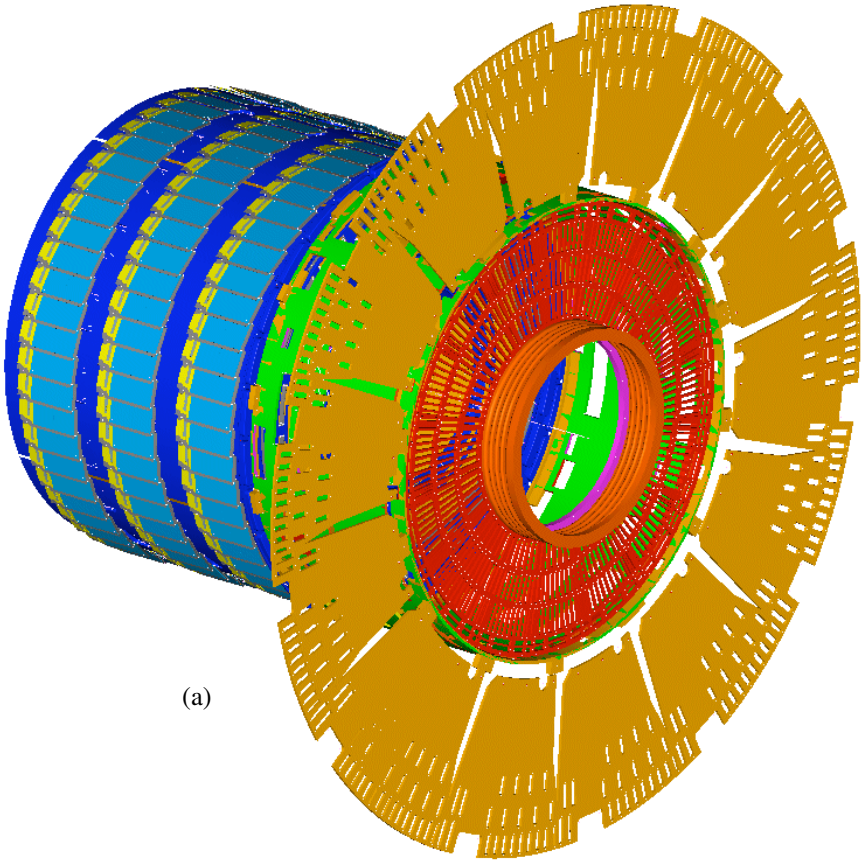

(a)

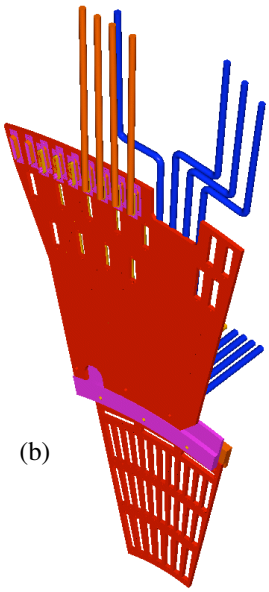

(b)

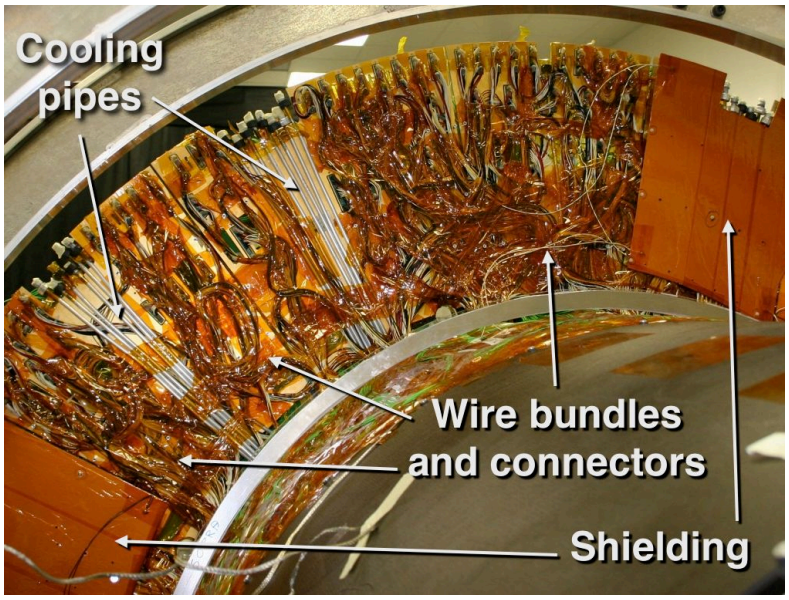

(c)

Figure 3: *(a) Schematic drawing of the TIB/TID+ sub-assembly. This structure and its counterpart (TIB/TID-) nests inside the Tracker Outer Barrel (TOB) one at each end. Services routed out from the margherita (in (b) a 3D drawing of a single petal is shown) consist of copper cables for powering (red tubes) and slow controls, optical fibres for signals and controls, and also cooling circuits (blue tubes). In (c) a photo of partially assembled petals is shown, where amongst the many wires the aluminium cooling pipes can be discerned.*

(max current $6\mathrm{A}$), and two separate high voltage (HV) regulators: $0 - 600\,\mathrm{V}$ (max current $13\,\mathrm{mA}$).

Each voltage regulator contains over voltage and over current hardware protections. Each HV regulator is fanned out (through jumpers) at the power supply back end into four lines, in order to provide more flexibility in the biasing scheme of different modules within the same power group. Two independent PSUs are mounted in a single unit (CAEN A4601H module).

Each control ring is powered by an individual $2.5\,\mathrm{V}$ regulator. Four control voltage regulators are hosted in one "control power supply module", CAEN A4602 board (during the integration phase, since A4602 modules were not available at the time, the $2.5\,\mathrm{V}$ line of one PSU was used to power each control ring). Up to nine power supply modules (A4601H and/or A4602) are hosted in one standard 6U high crate. All the regulators are "floating" (return line isolated from the local ground at the power supply module) and the LV regulators use sense wires to compensate for the voltage drop along the cable.

These power supplies were specifically developed [7, 8] for the Tracker and are characterised by their high degree of isolation: over $50\,\Omega$ up to $5\,\mathrm{MHz}$. Figure 4 shows the isolation measured on one power supply module.

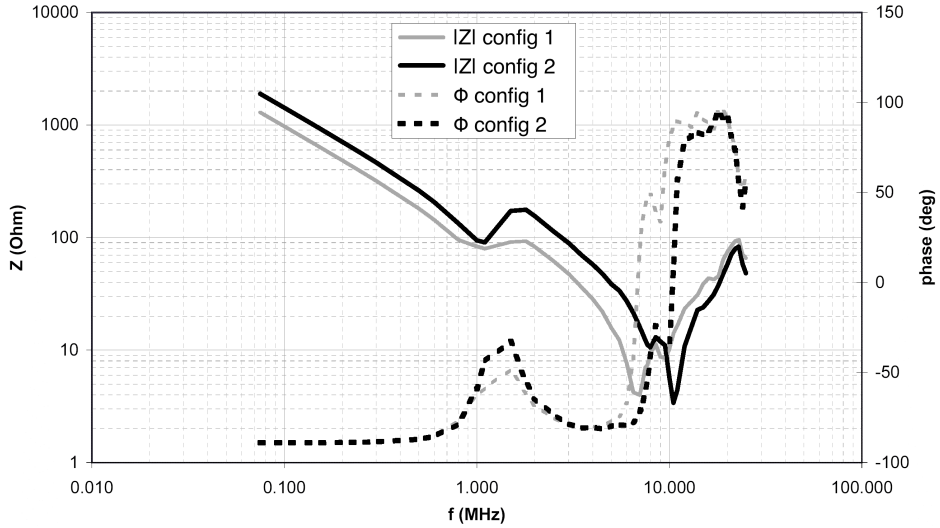

Figure 4: *Isolation between the RETURN line of the LV channels and the local ground on the rack for one power supply module. In "configuration 1" the PSU lateral panels are segmented and connected to different internal reference points, in "configuration 2" they are all connected to the local ground. The latter configuration was adopted for the final grounding scheme (see Section 3).*

According to the adopted powering scheme the reference voltage is fixed at the detector end; individual regulators supply independent voltages at the power supplies exit, according to the current consumption and the cable length attached to each line. The $1.25\,\mathrm{V}$ and $2.5\,\mathrm{V}$ regulators within the same PSU share the same return line. The cables used were also specially developed and are characterised by very low impedance. The length of the cables connecting the detector is of the order of 40-50 metres. Attention was paid, during the various phases of testing the system, as it grew from a few modules to a fully assembled shell, to have long cables powering the modules so as to reproduce final working conditions.

Many options remained concerning the choice of grounding scheme/filtering of these units. In Section 3 further details are given on how the PSUs were configured in the final setup.

2.3 The TIB/TID cooling circuits

The cooling circuits not only remove the heat generated by the electronics and the sensors, but also define the position of the modules. They are made of aluminium piping with $6\,\mathrm{mm}^2$ cross section and $0.3\,\mathrm{mm}$ thickness. These pipes are bent into loops and soldered to inlet/outlet manifolds, which connect several loops in parallel together. The thermal connection between pipes and silicon modules is made with aluminium ledges, which are glued with electrically isolating adhesive to the pipes. On each ledge there are two threaded M1 holes onto which the modules are tightened. Each cooling loop provides mechanical support for three detector modules in the TIB,

while for the TID the number is similar but varies depending on the disk. Figure 5 shows a partially dressed shell with the cooling circuits clearly evident.

From a grounding point of view we have three conductive elements (the loops, the ledges, and the carbon fibre shell) which are not in electrical contact even though they are in extremely close proximity to each other (a few microns of glue). This unusual electrical arrangement is due to the fact that for reasons of radiation hardness we could not use conductive glue. Also, because of the extreme thinness of the piping walls, it would have been very difficult and potentially problematic to use mechanical connections such as screws. And by the time the grounding scheme was being worked out the mechanical structures had already been produced and could not be easily modified.

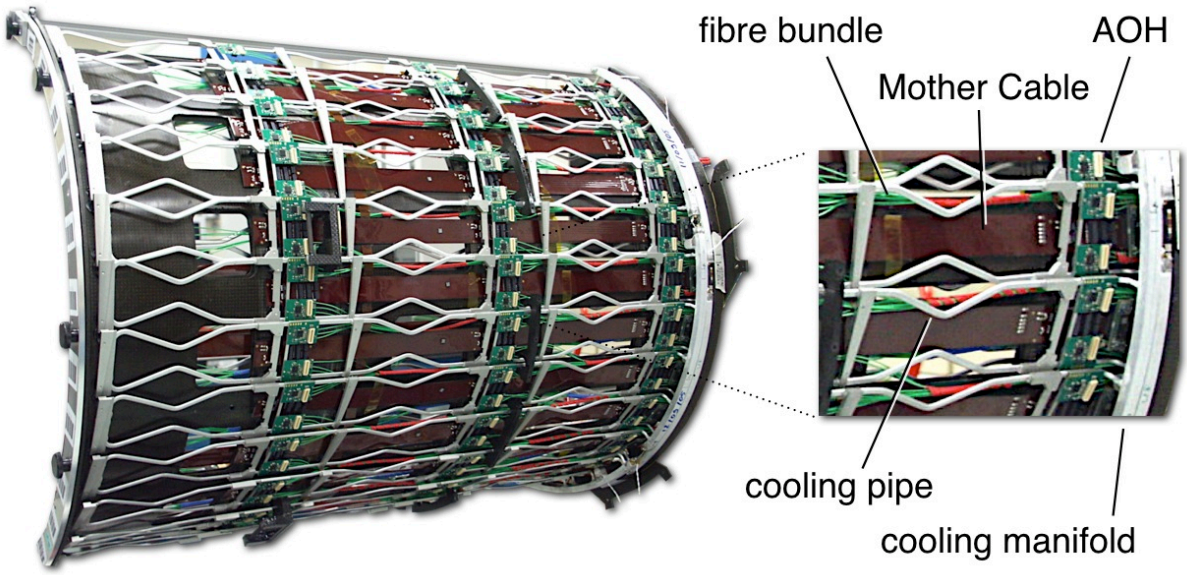

Figure 5: *A partially assembled Layer 1 shell inside one of the clean rooms in Florence used for TIB assembly. A series of aluminium cooling circuits can be seen glued to the carbon fibre structure. Just underneath the piping are the kapton inter-connect circuits (Mother Cables), which provide power and control signals to the detector modules. Also visible are the Analog Optical Hybrids (AOH), which transmit the detector module analogue output to the digitizers in the counting rooms.*

2.4 The TIB/TID control rings, power groups, and service distribution

Providing separate power and control lines for each detector module was not practical due to the cost and space requirements. For this reason all single detector modules have been electrically grouped together in small functional units. The basic group consists of the three modules that are mechanically fixed to a single cooling loop with a corresponding Mother Cable [9], which distributes power and control signals. The detector module powering has thus been parallelised, but without compromising reliability. In the two outer layers of the TIB and in the outermost rings of the TID, where single-sided modules are located[1)], the Mother Cables are further grouped together and have their LV power connectors joined in groups of two to four (power groups), extending the local ground to a more dispersed physical area. The LV sensing occurs either either at the interconnect end of the Mother Cable (Layer 1 and 2) or at most 20 cm away, depending on the particular grouping of detector modules.

Figure 5 shows the Mother Cables and the Analog Optical Hybrids (AOH), which electrically decouple the detector modules from the ADCs through the use of optical fibres. The control signals, distributed through the Mother Cable, actually come from another optically coupled module called the Digital Optical Hybrid Module (DOHM), which contains fibre receivers and transmitters for the clock and trigger. A detailed description of the TIB DOHM can be found in [10]. The DOHM provides these control signals to up to 15 separate Mother Cables each of which is equipped with a Comunication and Control Unit Module (CCUM) [11], which decodes the control signals (Fig. 6). The DOHM signal connections to the Mother Cable also connect together the various local return paths (grounds).

[1)] Single-sided modules have only 4 front end chips and thus have a much lower power consumption than double-sided ones, which have 12.

Thus the control ring structure itself, which embraces an even larger number of Mother Cables, contributes further to the "spreading" of the local ground. In order to keep things under control, two rules were established early on:

1. none of the previously described "power groups" should span more than one control ring;
2. control ring boundaries must stay within a single cooling circuit.

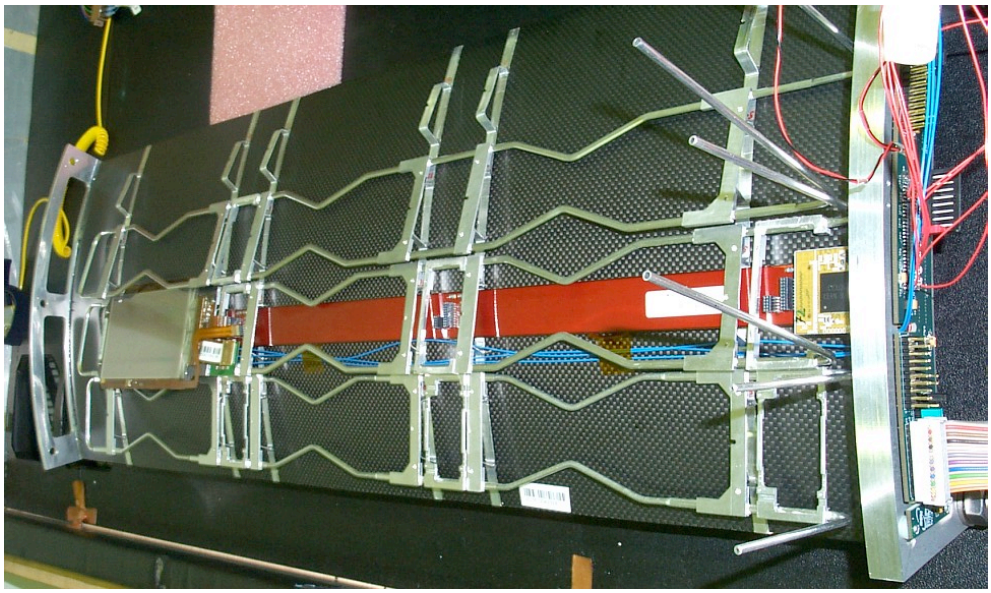

Figure 6: *A prototype TIB power group from 2003. Only one module has been mounted in the picture. This mock-up of what were to be the final shells was used to test various grounding schemes and evaluate the performance of the detector modules when powered in parallel. A CCUM can be seen plugged at the Mother Cable head at the right.*

The system conditions as stated so far are summarised in Table 1. Since the control signals are received at the DOHM via optical fibres and also the analogue data are sent back with other optical fibres, the whole system is electrically decoupled from the outside world. Thus the potential return paths are the power cables including their shields, the cooling pipes, and the carbon fibre structures.

Table 1: *System constraints*

1	Logical controls (clocks, triggers, monitoring) are optically decoupled (DOHM).
2	Data output is also optically decoupled (AOH).
3	Each Mother Cable constitutes an effective local ground where the LV return, the HV return and the control ring return are connected together.
4	Mother Cables can be further connected in parallel thus extending the local ground to up to four Mother Cables.
5	Each control ring connects the grounds of up to 15 Mother Cables together.
6	Control rings (DOHM + 4-15 CCUM) are powered independently from the detector module.
7	Power groups are contained inside control rings.
8	Control rings are contained inside cooling circuits.
9	Cable shields are terminated on the *margherita* at the detector end and with jumpers at the power supply side.
10	Power supplies are floating and provide a high degree of isolation at high frequencies ($50\,\Omega$ at $5\,\mathrm{MHz}$).

2.5 The TIB/TID detector module and its local ground structure

The last, but most important item that must be described from a grounding point of view is the detector module itself. The TIB/TID detector module (Fig. 7) includes a thin ($320\,\mu\mathrm{m}$) silicon sensor together with its front end electronics. The module is supported by a frame made of carbon fibre. A kapton circuit layer is used to isolate

the silicon and provide the electrical connection to the sensor back-plane, i.e. bias voltage supply and temperature probe readout. In addition, the module frame supports the front-end hybrid and the pitch adapter. Double-sided modules are obtained by gluing together a normal ($r\phi$) module with a modified module, where the sensor has been tilted by $100\,\mathrm{mrad}$ (stereo). A detailed description of the module assembly is given in [3] and [5].

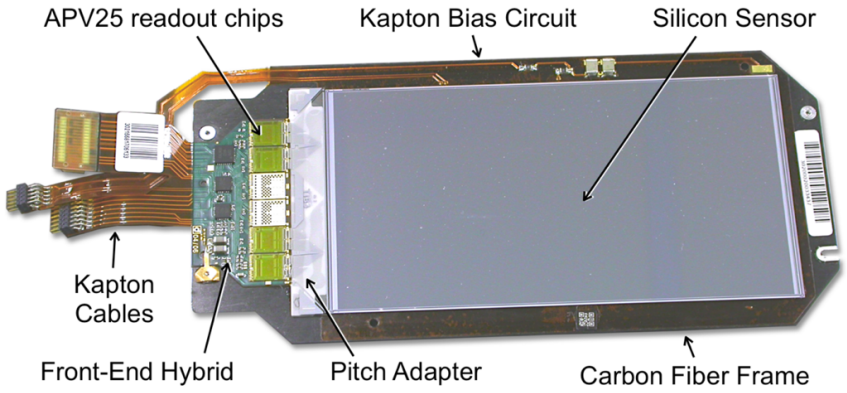

Figure 7: *The various components of a TIB module. A TID module apart from the wedge shaped sensor, has exactly the same components and layout.*

The detector front end chips, the APVs [12], have two different operating modes. A "slow" mode (*peak*), where the signal develops with characteristic times of $50 - 100\,\mathrm{ns}$, and a "fast" mode (*deconvolution*), where the original signal shape from the sensor is restored (time constants of the order of $25\,\mathrm{ns}$). At high LHC luminosity the chosen operating mode will be *deconvolution mode* as it allows pile-up effects to be disentangled. Because of weighting of multiple beam crossings, channel noise (pedestal RMS values) tends to be higher in *deconvolution mode*. The two modes do not show the same sensitivity to external pick-up noise. For example, a "quiet" setup can become "noisy" when switching from *peak* to *deconvolution* modes.

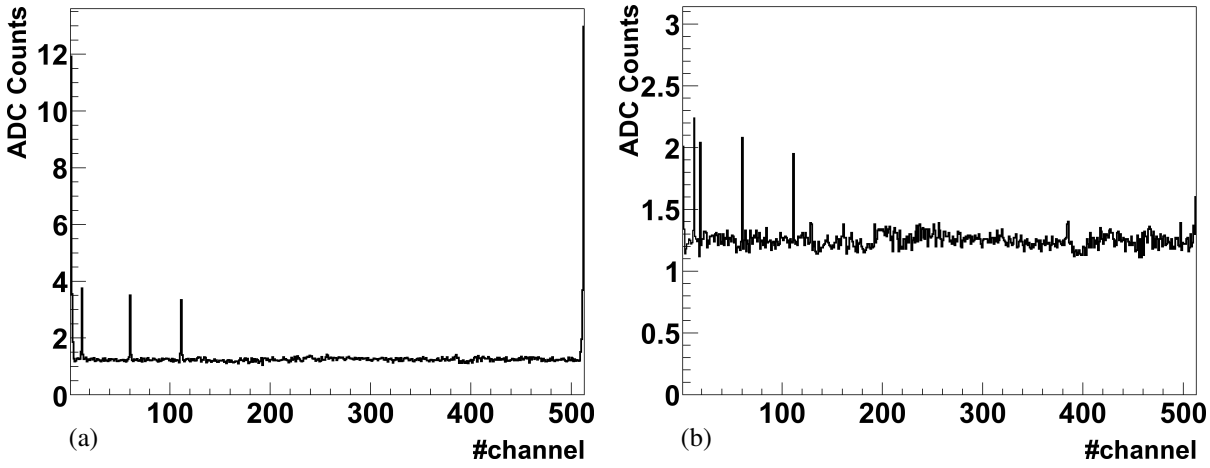

Figure 8: *Pedestal RMS (CM noise subtracted) vs. strip number for a 512 strip single-sided TIB module (peak mode was used because the effect is more evident): (a) no filtering, the edge strips (1-3 and 510-512) exhibit a much higher noise value (up to 12 ADC counts) than the rest; (b) finalised filtering, the edge strips exhibit now a more similar value to the rest and only the two outermost strips are still slightly affected.*

For what concerns the grounding of the module and its high voltage filtering, a solution was found that has proven to be very satisfactory. Figure 8(a) shows a plot for the pedestal RMS values of a prototype TIB module with 512 strips. Common Mode (CM) noise refers to a common pick-up disturbance that can be evaluated and subtracted out on an event by event basis in a straightforward manner, as long as the pick-up is of roughly the same intensity on all strips. The ARC based setup [1] for module post-production quality control was used.

The first and last groups of a few strips are distinctly noisier than the rest, up to the point of being unusable. This behaviour was typical of the first series production, until a modification was made to the design of the HV

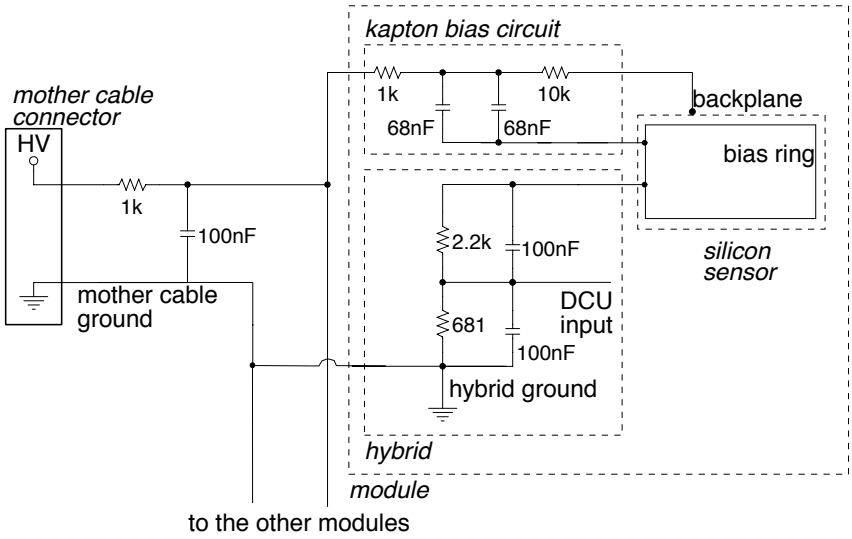

Figure 9: *HV biasing for the TIB/TID modules serviced by one Mother Cable. The T filters (on the kapton HV tail of each module) are grounded through the detector bias ring, which in turn is connected to the DCU circuit on the FE hybrid itself. The 100nF capacitors were added following the results shown in Fig. 8.*

filtering circuit (Fig. 9), specifically for TIB/TID modules. In fact, in the TIB/TID the kapton HV filtering circuit (a standard T type filter) is grounded through the detector bias ring and not with a separate dedicated copper trace. This is to prevent possible HV discharges on the kapton circuit (which is in very close proximity to the detector backplane) and also because in this way the blocking capacitors are very close to the detector, with only very short bonding wires for the connection. For this to work though, the bias ring must be shorted to the hybrid ground (which also coincides with the HV return). This clashed with the need to use the return of the bias ring as a probe to measure the detector bias current (by measuring the voltage drop across a resistor). A modification to the hybrid part of the circuit specific for TIB/TID was implemented so that the the bias current could be measured while at the same time achieving an optimal filtering.

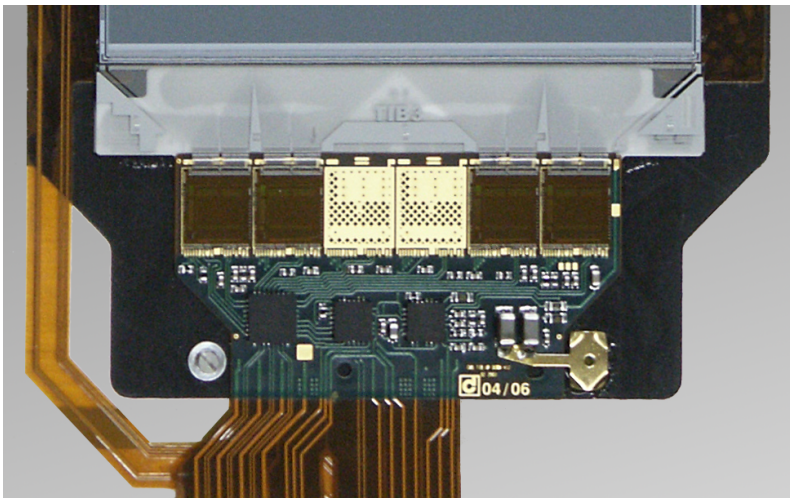

Figure 10: *A TIB hybrid bonded to the silicon sensor and with a cometa soldered to the two LV blocking capacitors (visible at lower right). The bent edges of the washer bite into the CF frame once the module is screwed down.*

The grounding of the module CF frame was also studied. This frame originally had been left floating with no electrical connection to the hybrid ground or indeed to any ground at all (the screws which fix the module to the aluminium cooling circuit are electrically isolated from the CF frame). It was shown that this made the module more sensitive to stray pick-up, which contributed to edge effects in the pedestal RMS distribution. In the end, a specially produced washer (*cometa*, Fig. 10) was used, which had a tail soldered to the hybrid ground (at the LV blocking capacitor pads) while its main body had sharp teeth that dug into the carbon fibre frame when the module

was attached to the cooling ledges.

The effectiveness of the *cometa* was first demonstrated by dedicated tests performed on a 512 strip single-sided module using the same setup mentioned before. Pick-up noise was injected in the detector module by leaving its aluminium carrier box floating instead of grounded as usual. As shown in Fig. 11 the *cometa* has a clear beneficial effect in reducing the noise tails at the APV edges.

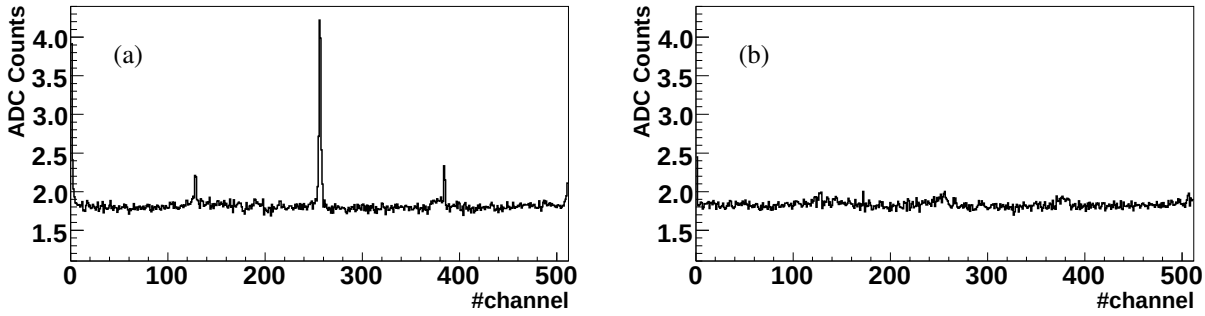

Figure 11: *The CM subtracted noise for a 512 strip TIB module measured with the module test setup (ARC) with the carrier left floating to have noise injection, without the cometa (a) and with the cometa (b). Deconvolution mode was used because it has a higher sensitivity to this type of noise pick-up.*

Further tests aimed to assess the grounding configuration of the double-sided module, which was subject to the following constraints: the *cometa* can be applied to the $r\phi$ module of the double-sided assembly as done on the single-sided module (i.e. $r\phi$ module frame referred to the local $r\phi$ module hybrid ground); there is no practical way to reference the stereo module frame to the stereo hybrid ground, i.e. a *cometa* like solution is not possible on the stereo module. On the contrary, it would be possible to reference the stereo module frame to the $r\phi$ hybrid frame via the $r\phi$ module frame shorting them by using an appropriate insert. Thus a more complicated setup was arranged to test a double-sided module. The setup allowed for any possible grounding configuration (not necessarily subject to the aforementioned constraints).

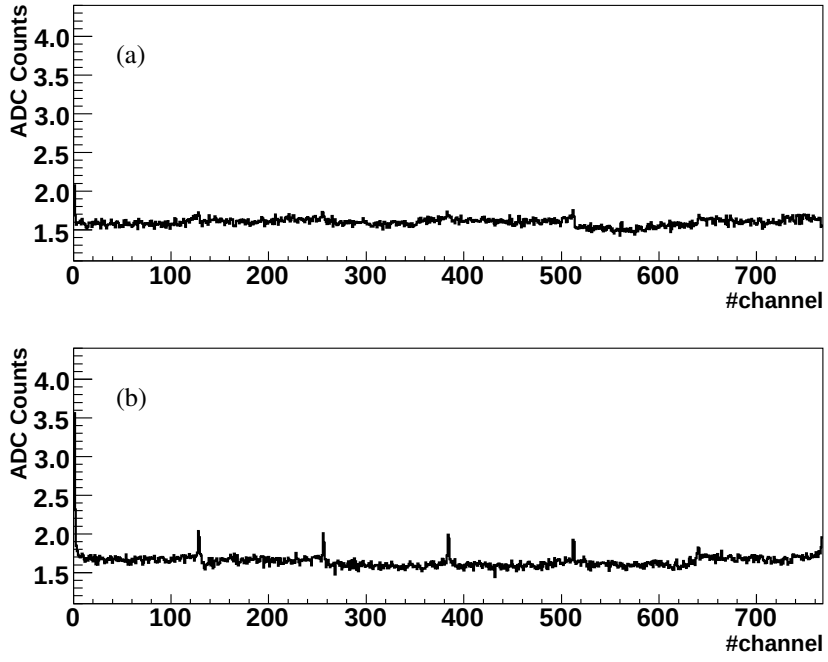

Figure 12: *The CM subtracted noise for a double-sided TIB module combination (deconvolution mode): (a) $r\phi$ module; (b) stereo module. The noise is measured with the module test setup (ARC) with the final grounding configuration (cometa on the $r\phi$ module).*

The results of the detailed test on this setup, again with noise artificially injected, can be summarised as follows. The *cometa*-like grounding of $r\phi$ module is confirmed to be largely beneficial for the $r\phi$ module noise itself (Fig. 12(a)), and marginally beneficial for the stereo module, which has the original grounding scheme with the floating carbon fibre frame (Figure 12(b)). The configuration in which the stereo module frame is referenced to the $r\phi$ hybrid is largely worse. The best noise figures are observed with the stereo module frame referenced to the stereo hybrid local ground, but this configuration is not viable.

As a consequence of these tests the following scheme was adopted: *cometa*-like grounding (frame referenced to the hybrid local ground) for single-sided modules; for double-sided assemblies, *cometa*-like grounding for $r\phi$ modules and design grounding (floating frame) for stereo modules.

3 General grounding and shielding criteria for TIB/TID

The TIB/TID connection to the experiment ground is made through the cooling pipes which, apart from the power cables, are the only metal conductors present in the tracker volume.

3.1 Detector grounding

Each of the four cylindrical layers has all of its cooling manifolds (which are fitted right at the end of the cylinder) electrically bridged together with short copper braids. These manifolds represent the corresponding layer ground point. All layers are shorted together during final assembly. A copper beryllium insert (*corona*) runs parallel to the aluminium manifolds and is soldered to them. This piece is used for all the ground connections that are necessary for the TIB and also to ground the CF cylindrical layer (Fig. 13) in a reproducible manner. A *corona* like ring is also used for the TID disks.

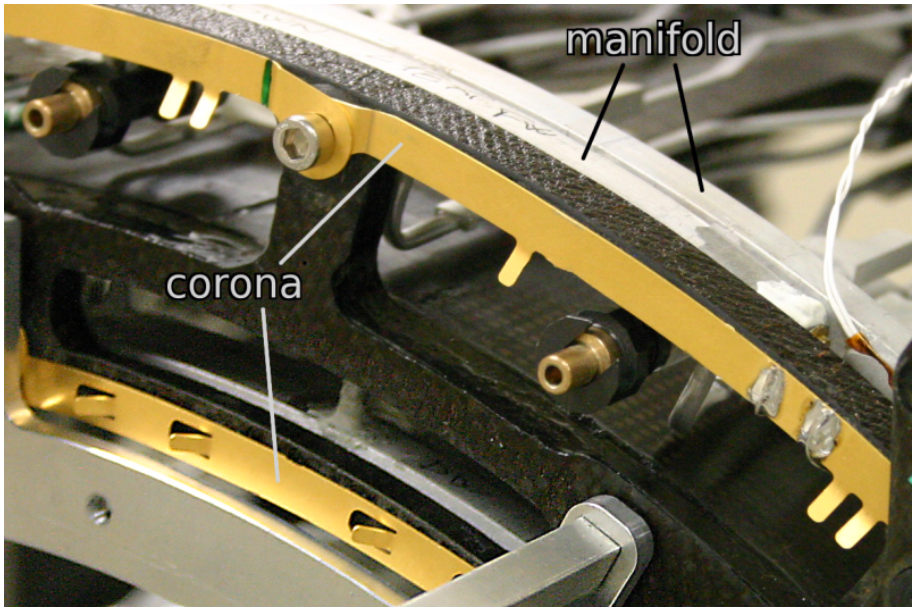

Figure 13: *Detail of the end part of one of the cylindrical layers of the TIB. At right, two aluminium cooling manifolds can be seen running along the cylinder CF end flange. On the other side of the flange the copper beryllium corona can be seen.*

The preliminary grounding scheme, for which the first results were obtained with the structure shown in Fig. 6, was to connect the ground of the Mother Cable and the ground of the DOHM on the *corona*, with the power cable shields, as stated at the beginning, connected to the *margherita*. The assembly of the shells thus followed the grounding guidelines summarised in Table 2.

3.2 The grounding of the power supplies modules

A4601H and A4602 modules require two $48\,\mathrm{V}$ input sources: the 48Vp ("power") for the voltage regulators and 48Vs ("service") for the control electronics, embedded hardware safety controls, and microprocessor. The 48Vp

Table 2: *First set of grounding rules for TIB/TID.*

1	Each half cylindrical shell (TIB) or disk (TID) has all of its cooling manifolds electrically connected together and to the *corona*.
2	All the Mother Cables have their common return (HV and LV) connected to the *corona*.
3	DOHMs and Mother Cables have a common return through the control signal cables.
4	All the DOHMs (which define the control ring structure) have their common return connected to the *corona* too.
5	Silicon detector modules are grounded through their electrical connection to the Mother Cable, and not directly through contact with the cooling circuit.
6	The *corona* also grounds the CF shell.
7	Internal cables are not shielded.
8	External power cable shields are connected to the *margherita*.
9	The ground is brought from the outside to the TIB/TID through the cooling pipes and through four copper braids per side, which run along the pipes.

and 48Vs are provided by AC/DC converters located on the same rack and distributed to each individual power supply module by the crate through dedicated $48\,\mathrm{V}$ rails.

The crate uses earth ground for its reference. The crates chassis, the earth ground, the rack structure, and the $48\,\mathrm{V}$ return lines are all connected together and define the local ground at the power supply end. A $47\,\mu\mathrm{F}$ capacitor is connected between each of the 48Vp, 48Vs positive lines and the local ground in order to provide some common mode filtering for the AC/DC converters. The chassis of the power supply modules (front panels, backplanes, and lateral panels) is also connected to the local ground (leaving the body of the power supplies unconnected to ground resulted in a slightly worse isolation of the channels). The external shield of the cables is not connected at the power supply end but only at the detector side.

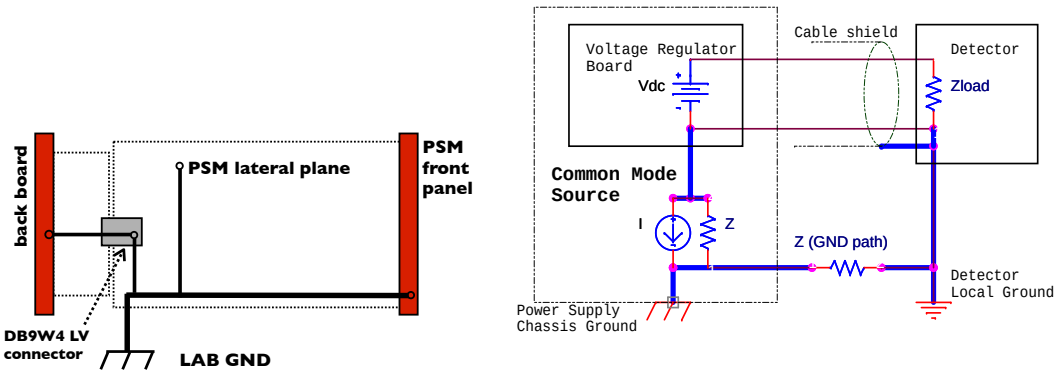

(a) (b)

Figure 14: *(a) Grounding arrangement for each A4601H unit (PSM is the module that houses two PSUs); the ground reference voltage is connected to a rail internal to the board, to which the body of the LV rear output connector (DB9W4), the front panel, the lateral plates, and the "back board" are connected (see text); (b) scheme representing the common mode current and the Z isolation impendance of the voltage regulators of the power supplies (see text).*

Figure 14 shows a sketch of the grounding arrangement adopted for each A4601H unit. The ground reference voltage is connected to an internal rail, to which the body of the LV rear output connector, the front panel, and the lateral plates are connected. Power cables are connected to interconnection output boards ("back boards"), placed at the back of the crate, which interface the power supply units to the cables, making it possible to remove the power supply modules without disconnecting the cables. The body of the back boards is also connected to the local ground, through the body of the board's LV power output connector.

Ideally, the LV regulators of all power supply units are electrically isolated from each other and from the rest of the world ("floating regulators"). In practice, the stray capacitance in the transformers will limit the level of isolation, particularly at higher frequencies. The impedance between the LV return line and the local ground (Z) quantifies the level of isolation achieved. The impedance Z was measured on a prototype PSM with an HP4285A LCR

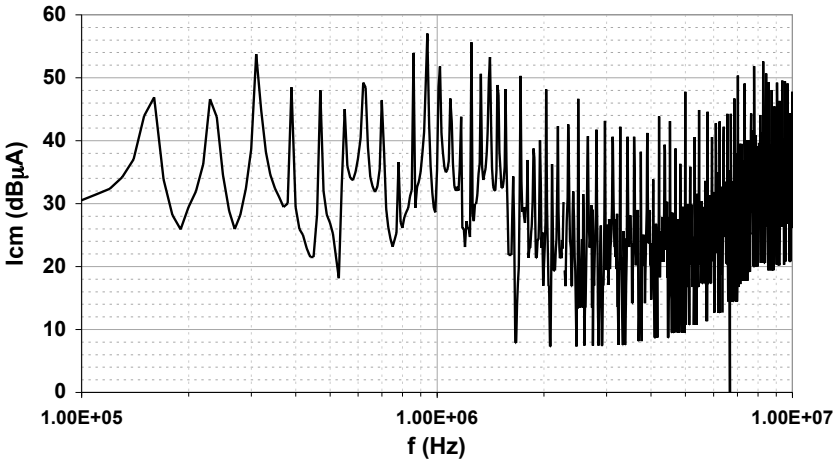

Figure 15: *Frequency spectrum of the current flowing from the return line to the local ground on the rack (common mode current) measured on one power supply with the final grounding configuration. Units are* $\mathrm{db}\mu\mathrm{A} = 20 \times \log(\mathrm{I_{CM}}/\mu\mathrm{A})$ *and* Hz.

meter capable of measuring the impedence up to $30\,\mathrm{MHz}$. These measurements have already been described in Section 2.2, where the functional dependence of Z on frequency is shown. The region of interest is 0.5 to $10\,\mathrm{MHz}$ as this is where the APV front end chip is most sensitive.

The power supplies transform the $48\,\mathrm{V}$ DC power to LV and HV using DC-DC switching regulators with $150\,\mathrm{kHz}$ base frequency. The LV and HV regulators feature a differential noise, measured at full load between the positive and negative electrodes, lower than $10\,\mathrm{mV}$ (LV) and $30\,\mathrm{mV}$ (HV) peak-to-peak spread. One general concern with switching supplies is the induction of spurious Common Mode currents ($\mathrm{I_{CM}}$) flowing through the regulators, the external load, and the connection to ground, at integer multiple frequencies of the fundamental. The common mode current can be depicted, as shown in Fig. 14(b), as due to a spurious current generator, of strength $\mathrm{I_{CM}}$ and internal impedence Z, placed between the LV lines and the local ground. The power supply units were also characterised with respect to the Common Mode current, by connecting the PSUs to resistive loads which simulate the configuration and the power consumption of the detector load. The LV return line at the output of the PSUs was connected to the rack's local ground through a $50\,\Omega$ resistor in parallel with the Z impedance. The voltage drop on the $50\,\Omega$ resistor ($\mathrm{V_{CM}}$) was monitored using a digital scope. The $\mathrm{I_{CM}}$ current, the ratio $\mathrm{V_{CM}}/(\mathrm{Z}||50\,\Omega)$, shown in Fig. 15, is four orders of magnitude less than the total output current of the regulators. Thus it is a negligible source of disturbance to the detector system.

3.3 Noise distributions

The first results obtained with up to 12 modules and one control ring on prototype structures were very promising (Fig. 16). The data was acquired with the APVs in *deconvolution mode*. A prototype of the experiment FED [13] was used for the ADCs, although the gain of the ADCs was lower than those in the experiment version. These ADCs are different from the ones used in the ARC setup, so the absolute noise values are not comparable to those in the previous plots.

From the plots no immediate evidence of pick-up noise can be seen, or of any cross-talk between modules. These results gave the first indications that the adopted scheme was robust. These results were then further confirmed when the first assembled half shells were tested and all the modules were read out at the same time (Fig. 17). These tests were performed in Pisa at the TIB Burn-In facility [14], where the final DAQ electronics was installed with an adequate number of channels. The final ADCs have a factor four more sensitivity, which explains the change in the RMS values from the previous plot. Although a few outliers can be seen on the logarithmic scale of the plot, 99% of the strips are well behaved and within specifications.

As will be described in the next section, further improvements were implemented and these all but eliminated residual high noise tails.

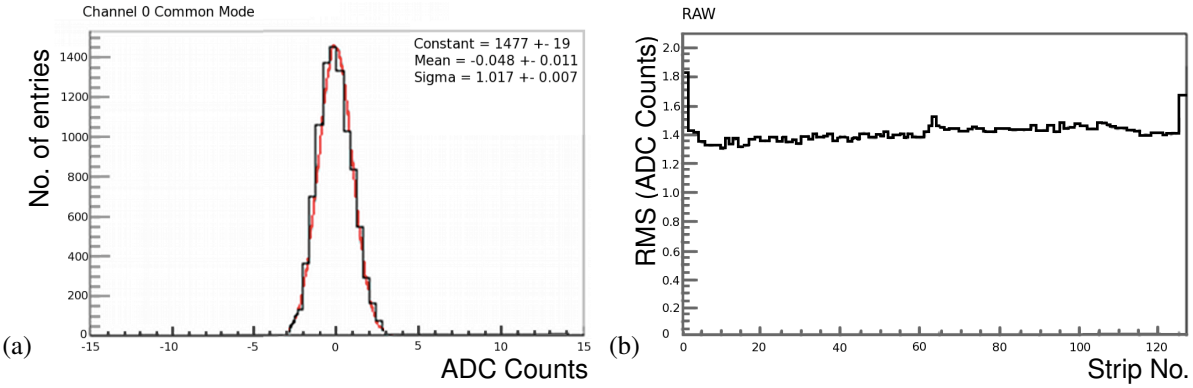

Figure 16: *(a) Common mode noise of a TIB module installed on prototype structure with the grounding scheme as described in the text; (b) pedestal RMS profile of one chip (128 strips, deconvolution mode) of a TIB module installed on prototype structure with the grounding scheme as described in the text. One ADC unit roughly corresponds to 700 electrons.*

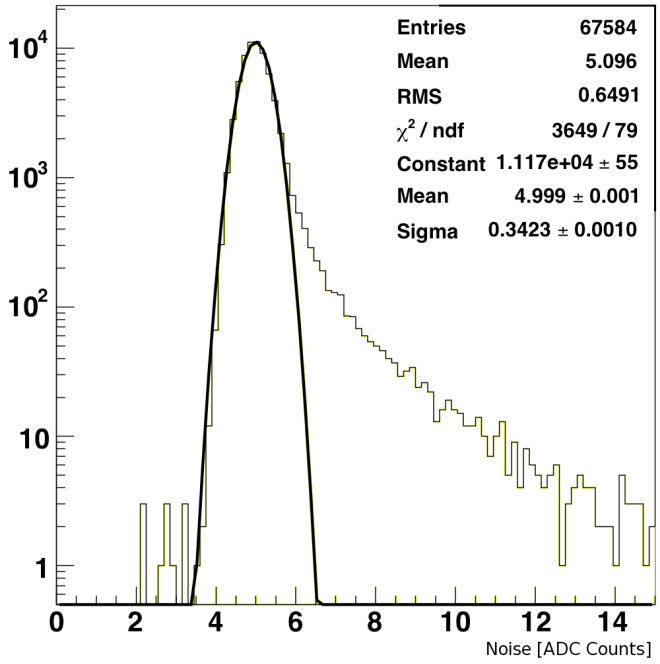

Figure 17: *Strip pedestal RMS (CM noise subtracted, deconvolution mode) distribution for a TIB Layer 3 assembled half shell. Out of a total of 67584 strips only a few hundred show a noisy behaviour. See text for the ADC scale used.*

4 Evolution of the grounding criteria

The noise performance in the very first TIB/TID burn-in runs was in general quite satisfactory (Fig. 17), but showed irreproducible excess noise in some modules. While most modules had a perfectly flat RMS profile (versus strip number), in some cases clear peaks were seen with a wave like structure of the profile (Fig. 18), even after CM subtraction.

For single-sided modules the noise excess was more evident on the boundary between the 1st and 2nd APVs and between the 3rd and 4th APVs (around strip 130 and strip 390). For double-sided TIB modules, the noise was highest between the 2nd and 3rd and between the 4th and 5th APVs. This corresponds to the position of the cooling pipes under the sensor (and the pitch adapter).

The only reproducible feature seemed to be that modules close to the end-flange (where the DOHM and CCUM are located) were more badly affected. Otherwise, the noise peak could vanish or double from one run to the next. Initially, the answer was to carefully shield all digital activity on the DOHM and, at a later stage, the end of the signal cable that carries the signals from the DOHM to the CCU on the interconnect end the Mother Cable. The

shielded flat cables can be seen in Fig. 19. The shields were connected to the *corona*. These yielded only marginal improvements and did not eliminate the observed noise patterns.

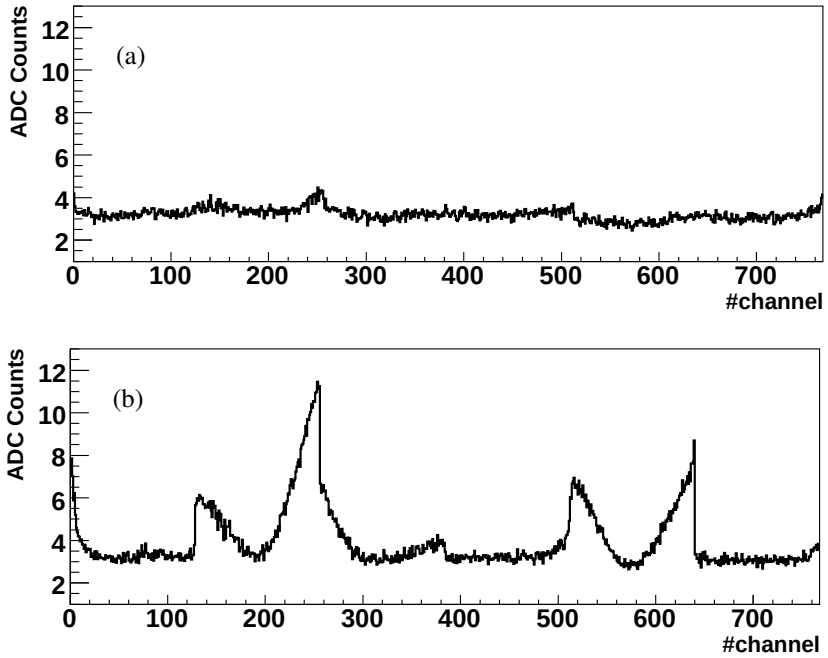

Figure 18: *Strip pedestal RMS vs strip number (CM noise subtracted, deconvolution mode) for a TIB Layer 2 stereo module in two different data taking runs: the run represented in (a) does not show the noise patterns visible in (b).*

At the same time an investigation on the electrical isolation of the cooling ledges from the cooling pipe was carried out. In many cases it was found that, not withstanding the use of anodised aluminium and electrically insulating glue, some of the ledges were shorted to the pipe. Since the cooling ledge is by design connected to the FE hybrid

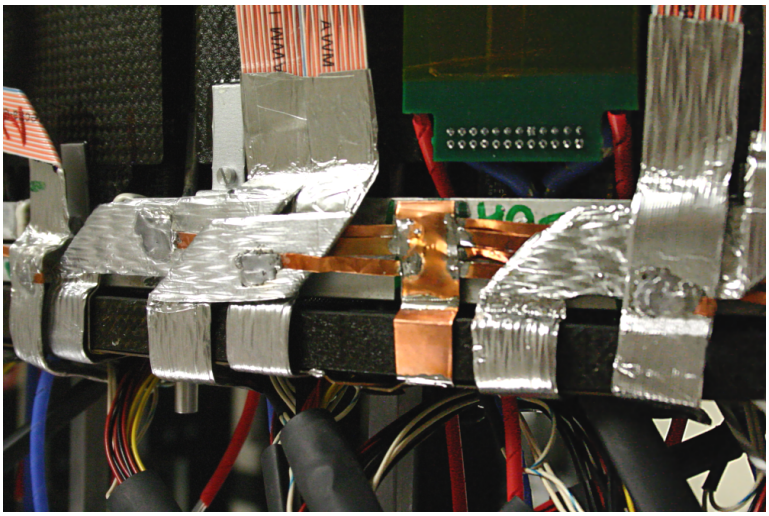

Figure 19: *Partial shielding of the control ring cables in proximity of the end flange. These cables carry clock (*40 MHz*) and trigger information.*

return, the situation from the electrical point of view was somewhat undefined (Fig. 20), as some of the cooling circuits would carry the string return current through these unwanted connections.

It was soon evident though that these "shorts" could not be removed, and so they were all mapped for every half-shell. At the same time an investigation was begun on the relationship between the shorts and the observed noise patterns both with "traditional tools" (oscilloscope) and with software analysis programs which had graphical outputs capable of simultaneously displaying possible correlations between power groups, control rings, and other

groupings of modules (Fig. 21).

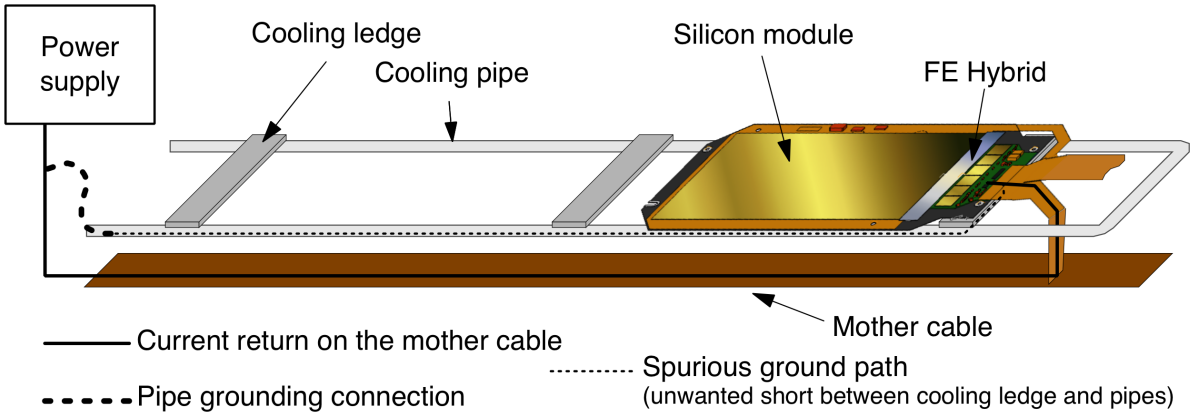

Figure 20: *Schematic diagram of a cooling circuit, showing potential ground loops. These come about through unwanted electrical connections between the cooling ledges and the cooling circuit aluminium pipes.*

In addition to pedestal RMS other quantities were checked for correlations with the trigger and clock. From these studies two things emerged:

1. although the noise emergence was not repeatable from run to run, some module strings seemed more affected than others (i.e. they would show noisy patterns more often than most);
2. a 20 MHz noise was present on the corresponding cooling tube (measured respect to the FE hybrid return) every time the noisy patterns appeared (Fig. 22).

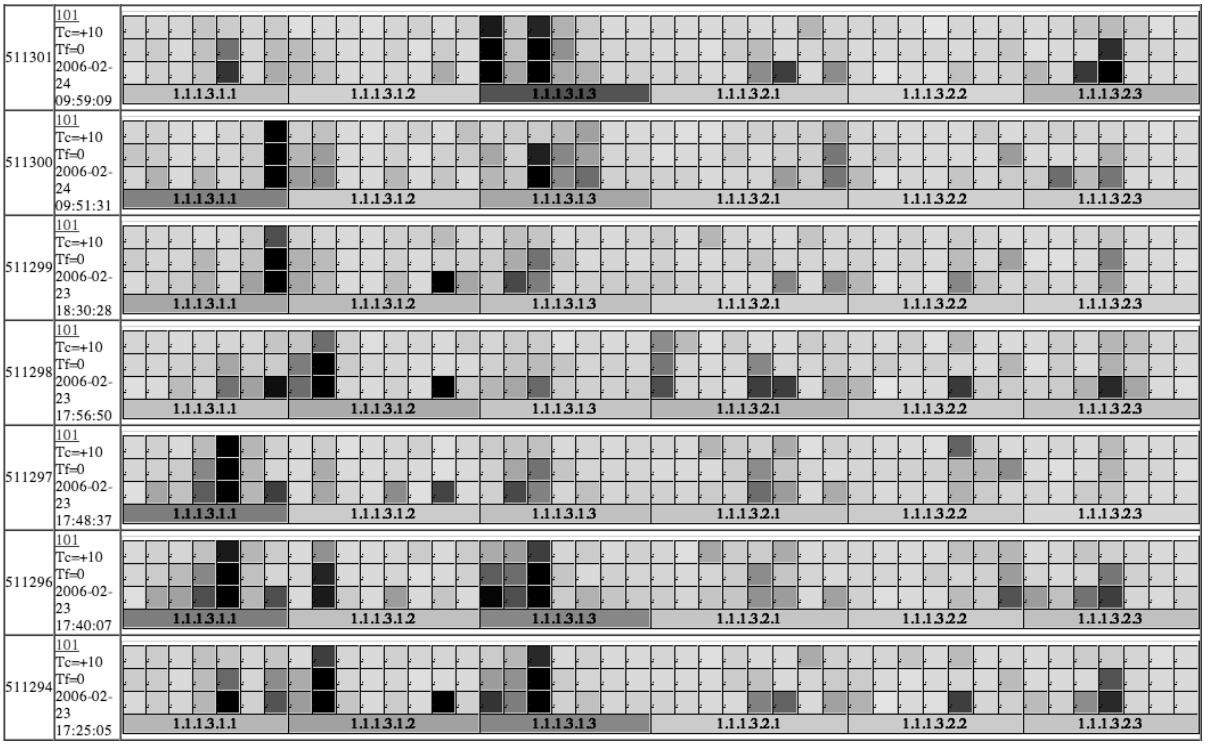

Figure 21: *Graphical output from the noise analyzer software. Each major row corresponds to a different run. Each detector module is visible as a greyed square organised in strips of three (Mother Cable pattern). Darker grey levels indicate anomalous noise conditions.*

The oscilloscope measurements were made in differential mode using low capacitance active probes. At this point the mechanism by which these noise patterns could appear was evident. Since the FE electronics samples the charge on the strips at 40 MHz, a 20 MHz pick-up would (depending on the phase relative to the 40 MHz sampling

clock) be seen either as a positive or a negative charge injection. A detailed analysis of the data with the software analyzer using special trigger configurations confirmed this see-saw mechanism which affected individual strips in different ways thus invalidating the CM subtraction algorithm. The question remained as to its origin and of why it was not always present.

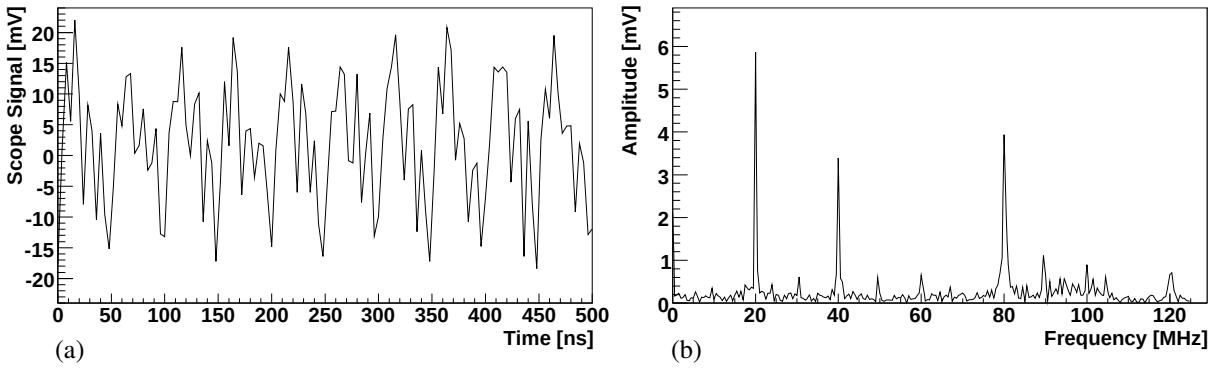

Figure 22: *(a) Pick-up noise as seen on an oscilloscope with an evident* $50\,\mathrm{ns}$ *periodic pattern; (b) the FFT spectra of the pick-up noise.*

The answer to these questions lies in a little known feature of the control rings. The data links in the control rings use a NRZI (Non Return to Zero with Invert 1 on change) coding. Thus a transition represents a logical one and an absence of transitions represent a logical zero (Fig. 23).

Since a control ring handles a large number of modules, provisions have been made in case of a single point failure along the ring. Thus all CCUMs have duplicate inputs and outputs (redundancy). In normal operation only one output is active (A output) while the redundant output (B output) transmits idle patterns [11]. Unfortunately this idle pattern corresponds mainly to a series of 1s which, given the encoding used, resembles a $20\,\mathrm{MHz}$ clock. This explains the origin but not why it sometimes disappears. Again one has to bear in mind the exact behaviour of these outputs. Normally the A output will also transmit idle patterns. These can be either in phase or 180 degrees out of phase with those present on the B output. The phase choice of the B (redundant) output is randomly determined at the start of run when a CCUM reset is performed. So at every run, every single CCUM of the ring can have its two outputs either interfering constructively (maximum disturbance) or destructively (minimum disturbance).

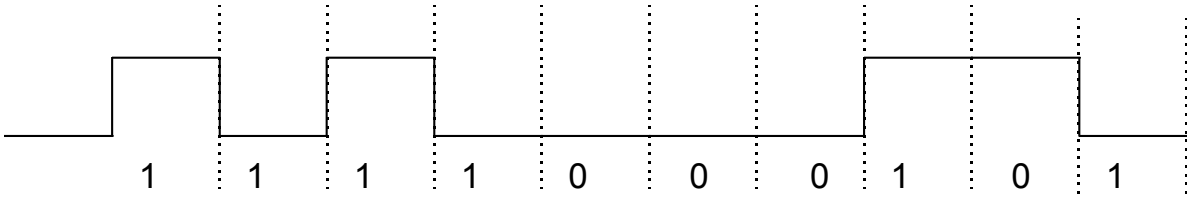

Figure 23: *NRZI coding used for the control ring data links. These are sampled with the* $40\,\mathrm{MHz}$ *clocks.*

Having thus identified the noise source and its irreproducibility, several grounding configurations between cooling circuits, detector modules, and DOHM were tested for the various TIB layers. Both the *corona* and the ground connection through the DOHM reduced the sensitivity to the $20\,\mathrm{MHz}$ pick-up for single-sided layers, where the power groups span up to four different Mother Cables.

In double-sided layers the situation was more complex: there the noise performance was best when the ground connections between Mother Cable and cooling manifolds were removed.

The final solution, though, was only determined once the mapping of the ledge to cooling tube shorts was finished. At that point a correlation emerged between strings where a cooling ledge was in electrical contact with a cooling tube and noise susceptibility of the string itself. Or, more accurately, an anti-correlation emerged. In fact, as already observed, some of the strings seemed immune to these “wavy” noise patterns. By comparing with the map it became evident that the short between cooling ledge and cooling tube had a very beneficial effect of completely eliminating the pick-up noise. Thus it was decided to short all the FE hybrids of the end modules on the strings to the cooling tubes. This was done (Fig. 24) by soldering with a special solder etch which allowed tin to bind on our aluminium cooling tubes. Thus for every string of the TIB, the end module was soldered. This together with the

shielding mentioned before yielded exceptionally good results, which were also stable in time and did not depend on run conditions.

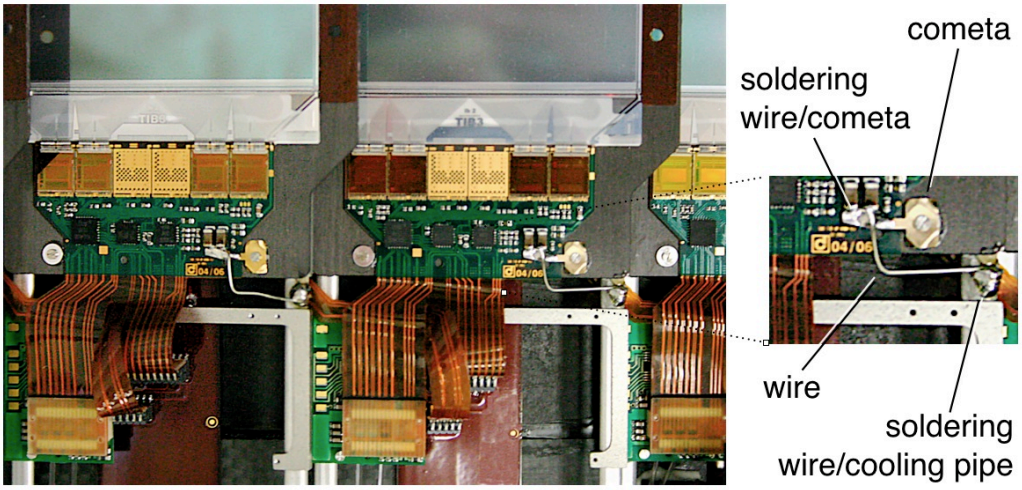

Figure 24: *The connection between FE hybrid and cooling circuit. The connection is soldered to the cometa and to the aluminium tube, which is just visible beneath the hybrid.*

In Fig. 25 the same type of plot is shown as in Fig. 17. Now the number of badly behaving strips is a handful at most, and all modules present a regular pedestal RMS profile with no wavy structure.

Table 3 summarises the updates to the prescriptions that were used for TIB grounding and shielding. Actually the situation with the TID is more subtle. Given the ring geometry, the ground connections between cooling circuit and the Mother Cable are achieved through a thin copper braid that runs around the full perimeter of the disks. Also, the DOHM is connected to the cooling manifolds as well.

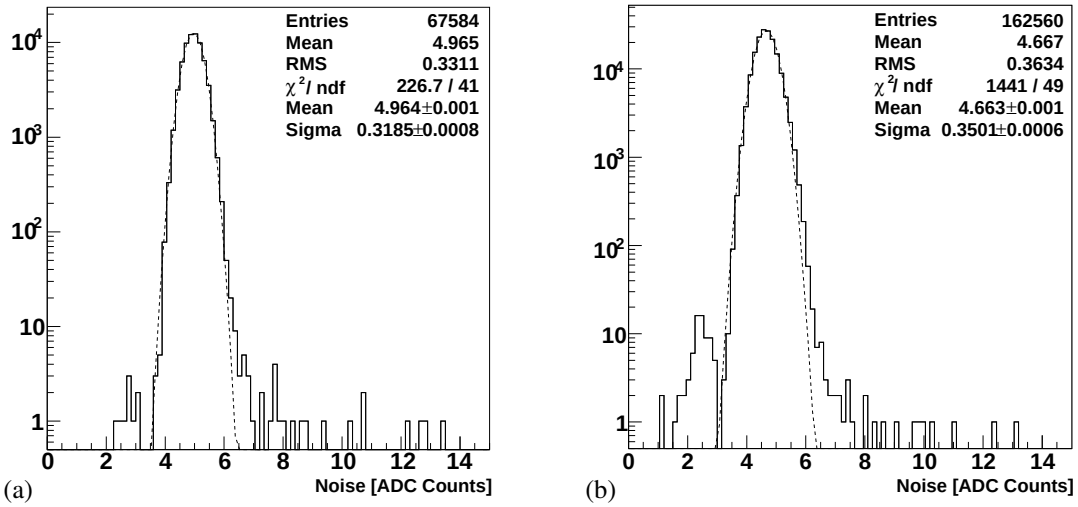

Figure 25: *(a) Pedestal RMS (CM noise subtracted, deconvolution mode) distribution for the 67584 strips of a TIB Layer 3 half shell in the final grounding and shielding configuration (to be compared with Fig. 17); (b) pedestal RMS (CM noise subtracted) distribution for a ϕ slice of the TIB+, consisting of two control rings in Layer 1 and 2 and a control ring in Layer 3 and 4.*

While the qualitative features of the excess noise observed in the TIB were found in the TID as well, its effect was much less pronounced. This reduced sensitivity is probably due to the different orientation of the cooling pipes with respect to the read-out strips (the pipes under the sensor are nearly perpendicular to the strips and not parallel as in the TIB). Therefore, the additional grounding contact between cooling pipe and FE hybrid ground was not adopted for the TID.

Table 3: *Update, for TIB only, to the set of grounding rules of Table 2.*

4a	Modification of rule 4: the end module of a string has a direct soldered connection between the module ground and the cooling pipe.
6a	Modification of rule 6: control ring cables and the DOHM have a partial shielding in place.

5 Global noise performance and reproducibility

Following the final assembly, the two halves of the TIB/TID were shipped to CERN where they were inserted inside the Tracker Outer Barrel and their electrical, optical, and cooling services were integrated within the Tracker structure.

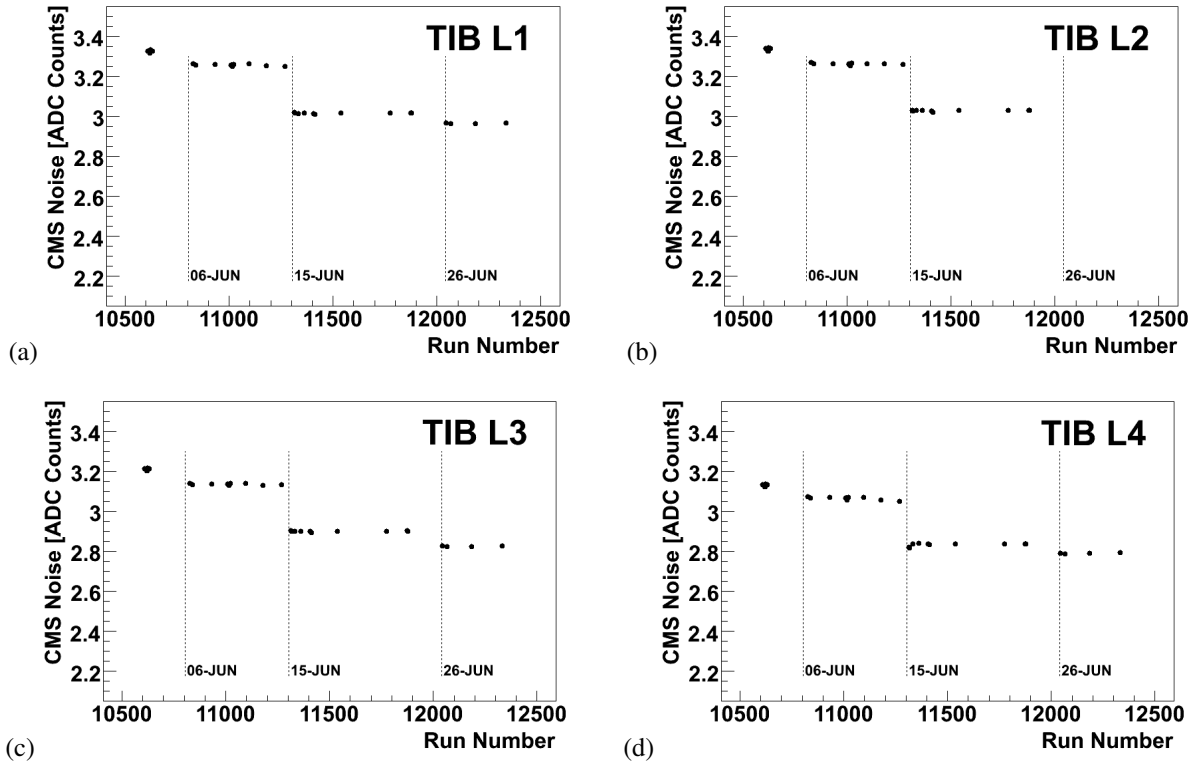

Figure 26: *Average noise values for TIB layers as a function of run number. The overall stability was excellent. The runs were performed over a period of nearly a month at different temperatures and, correspondingly, APV parameter settings. The APVs were set in peak mode.*

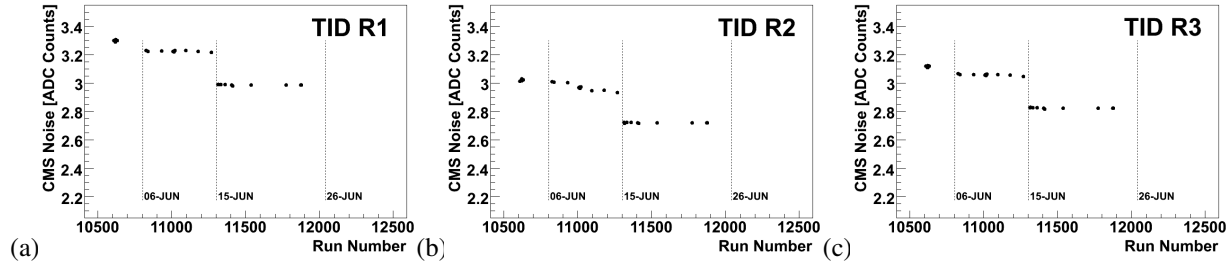

Figure 27: *Average noise values (peak mode) for TID rings as a function of run number. Just as for TIB, the overall stability was excellent.*

Before the installation of the SST in the CMS experiment, the performance of 15% of the detector, equally shared between TIB/TID, TOB, and TEC, was studied by collecting about 4.5 million cosmic ray triggers at the Tracker Integration Facility (TIF) [15]. In this period the pedestal and the noise of each channel were measured regularly. Figures 26 and 27 show the fitted mean values of the strip common mode subtracted noise for each TIB layer and TID ring, respectively, as a function of the run number. The displayed range corresponds to about one month; the sudden changes correspond to the changes of the APV parameter settings due to the change of the coolant

temperature from $10^{\circ}\mathrm{C}$ to $0^{\circ}\mathrm{C}$, $-10^{\circ}\mathrm{C}$, and $-15^{\circ}\mathrm{C}$. In this period the APVs were operated mainly in *peak mode*: this explain the different absolute noise value with respect to the values in Figs. 17 and 25.

During these tests at the TIF the noise performance of the fully integrated Silicon Strip Tracker was studied also with a dedicated setup. An oscillator was inductively coupled to the power cable of one TIB Layer 3 power group (4 strings, 12 modules).

First the strips noise was measured without the oscillator as reference, and then three different measurements with increasing amplitude of the injected oscillating signal were performed: 85 dB μV at $10\,\mathrm{MHz}$, 100 dB μV at $10\,\mathrm{MHz}$, and 100 dB μV at $15\,\mathrm{MHz}$ [16]. Figure 28 shows the measured CM subtracted noise for each strip in those 12 modules with no injection (top), with the largest injected signal (middle) and the difference between the two measurement. No sensitivity to the injected signal was observed.

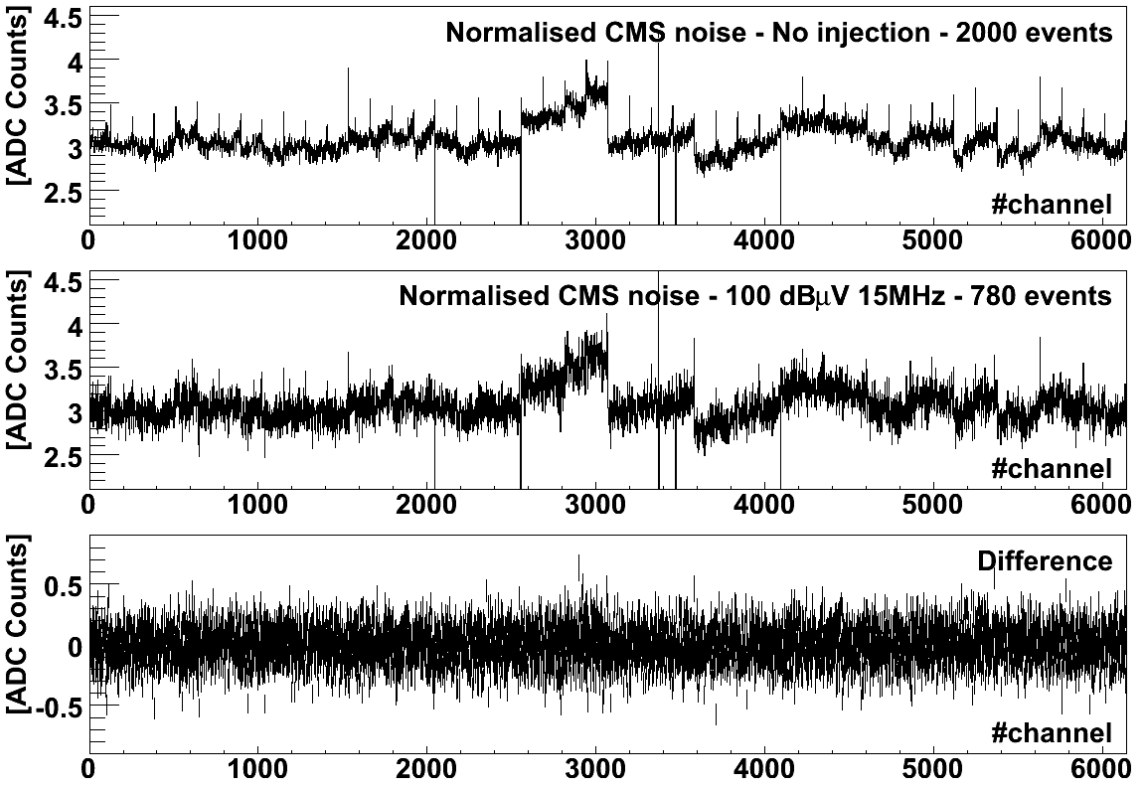

Figure 28: *Strip noise profiles with and without injection of an oscillating signal in the power cable.*

6 Conclusions

The grounding and shielding of the TIB/TID was a complex undertaking that was started as soon as the first detector modules became available. Even so, all the effort put in the enterprise only started providing stable results once the final assemblies were ready. This underlines how complex the various interactions between all the components can be.

The software tools developed for the job and the expertise of the people involved has resulted in a tracker that has excellent noise performance.

The results shown in this paper have later been confirmed when the tracker was finally installed inside the magnet at the interaction point with full blown tests in P5 together with the other sub-detectors.

References

[1] S. Albergo et al., *Test of the Inner Tracker Silicon Microstrip Modules*, CMS Note 2009/001.

[2] L. Borello, E. Focardi, A. Macchiolo, A. Messineo, *Sensor Design for the CMS Silicon Strip Tracker*, CMS-NOTE-2003-020.

[3] The CMS Tracker Collaboration, *The Tracker Project Technical Design Report*, CERN-LHCC-98-06 (1998).

[4] The CMS Tracker Collaboration, *Addendum to the Tracker Project Technical Design Report*, CERN-LHCC-2000-016 (2000).

[5] The CMS Collaboration, *The CMS experiment at the CERN LHC*, JINST 3 S08004 (2008).

[6] CAEN S.p.A., Via Vetraia 11, 55049 - Viareggio (LU) - Italy, http://www.caen.it

[7] A. Bocci, R. D'Alessandro, S. Paoletti, G. Parrini, *The Powering Scheme of the CMS Silicon Strip Tracker*, proceedings of the 10^{th} Workshop on electronics for LHC and future experiments, CERN-2004-010, CERN-LHCC-2004-030 (2004).

[8] S. Paoletti, *The implementation of the power supply system of the CMS silicon strip tracker*, proceedings of the Topical workshop on Electronics for Particle Physics, TWEPP-07, CERN report CERN-2007-007, (2007) 377.

[9] R. DeRobertis et al., *The Mother Cable for the Tracker Inner Barrel* , in process of publication.

[10] R. Benotto et al., *Design and test of the digital opto hybrid module for the CMS tracker inner barrel and disks*, CMS Note 2008/013 (2008).

[11] C. Paillard, C. Ljuslin and A. Marchioro, *The CCU25: a network oriented communication and control unit integrated circuit in a* $0.25\,\mu\mathrm{m}$ *CMOS technology*, proceedings of the 8th Workshop on Electronics for LHC Experiments, Colmar, France (2002) and references therein.

[12] M.J. French et al., *Design and results from the APV25, a deep sub-micron CMOS front-end chip for the CMS tracker*, Nucl. Instr. and Meth. A 466 (2001) 359.

[13] J. Coughlan et al., *The CMS tracker front-end driver*, in Proceedings of the 9th Workshop on Electronics for LHC Experiments, Amsterdam, The Netherlands (2003).

[14] M. D'Alfonso et al., *Validation tests of the CMS TIB/TID structures*, in process of publication.

[15] W. Adam et al., *Silicon Strip Tracker Detector Performance with Cosmic Ray Data at the Tracker Integration Facility*, CMS Note 2008/032 (2008).

[16] Private communication to the authors.